

Deterioration of Trabecular Architecture in Hypogonadal Men

MARIA BENITO, BRYON GOMBERG, FELIX W. WEHRLI, RICHARD H. WEENING, BABETTE ZEMEL, ALEXANDER C. WRIGHT, HEE KWON SONG, ANDREW CUCCHIARA, AND PETER J. SNYDER

Departments of Medicine (M.B., P.J.S.), Radiology (B.G., F.W.W., R.H.W., A.C.W., H.K.S.), and Bioengineering (B.G.), University of Pennsylvania; General Clinical Research Centers (B.Z.), Children's Hospital of Philadelphia; and Hospital of the University of Pennsylvania (A.C.), Philadelphia, Pennsylvania 19104

Bone strength depends on trabecular architecture, characterized by interconnected plates and rods. In osteoporosis, the plates become fenestrated, resulting in more rods that deteriorate and become disconnected. In men, hypogonadism is a common cause of osteoporosis. To determine whether male hypogonadism affects trabecular architecture, we selected 10 men with severe, untreated hypogonadism, and for each hypogonadal man, we selected a eugonadal man matched for race and age. Trabecular architecture in the distal tibia was assessed by magnetic resonance microimaging. Two composite topological indices were determined: the ratio of surface voxels (representing plates) to curve voxels (representing

rods), which is higher when architecture is more intact; and the erosion index, a ratio of parameters expected to increase upon architectural deterioration to those expected to decrease, which is higher when deterioration is greater. The surface/curve ratio was 36% lower ($P = 0.004$), and the erosion index was 36% higher ($P = 0.003$) in the hypogonadal men than in the eugonadal men. In contrast, bone mineral density of the spine and hip were not significantly different between the two groups. We conclude that male hypogonadism is associated with marked deterioration of trabecular architecture and to a greater degree than bone densitometry of the spine and hip suggests. (*J Clin Endocrinol Metab* 88: 1497–1502, 2003)

OSTEOPOROSIS IS A MAJOR public health problem in men (1) as well as in women. The lifetime risk of osteoporotic fractures in men has been estimated to be 13–25% (2, 3), and the mortality from fractures in men has been estimated to be as high as 30%, which is higher than in women (4, 5).

A major cause of osteoporosis in men is hypogonadism. Among men evaluated for osteoporosis, 5–30% have no apparent cause other than hypogonadism (6–9). Among men evaluated for hypogonadism, bone mineral density is lower than that in eugonadal men, by 17% in one study by single photon absorptiometry of the distal radius (10) and 9% in another study by dual energy x-ray absorptiometry of the lumbar spine (11). When men are made hypogonadal by orchietomy (12) or GnRH agonist treatment (13–15), their bone mineral density decreases, and when hypogonadal men are treated with replacement doses of testosterone, their bone mineral density increases (11, 16–18).

Current methods for assessing osteoporosis have major limitations. Although bone densitometry is noninvasive and the results correlate with existing vertebral deformities (19) and the development of clinical fractures (20), the correlation is imperfect. In addition, subjects who have similar bone mineral density measurements may have different degrees of perturbation of bone architecture as determined by histomorphometry (21–23), and some therapeutic agents produce large decreases in fracture incidence although they produce

only small increases in bone mineral density (24, 25). These discrepancies may reflect the failure of bone densitometry to discern the turnover of bone (26) and the effect of turnover on microarchitecture. Analysis of bone biopsied from the iliac crest can determine bone architecture directly, and it is from such biopsies that the concept was developed that osteoporosis involves deterioration of trabecular plates to become rods that thin and become disconnected (27). The invasiveness of bone biopsy, however, is not only a deterrent; the physical removal of the bone to be assessed precludes repeat assessment of the same bone.

Because of the limitations of these techniques and yet the importance of the microarchitecture of bone in determining its strength and resistance to fracture, several new, noninvasive techniques to assess bone architecture have been developed, including those based on quantitative computed tomography (CT; Refs. 28–30) and magnetic resonance imaging (31–34). High-resolution magnetic resonance microimaging (μ MRI) permits the *in vivo* acquisition of images at resolutions high enough to discern individual trabeculae (35), so that the characteristics of bone microarchitecture and the parameters that reflect the integrity of the trabecular network can be quantitated (36, 37). This technique, termed the virtual bone biopsy, has been shown to differentiate women who have vertebral deformities from those who do not better than bone densitometry (38).

The specific aim of this study was to determine the effect of male hypogonadism on the trabecular microarchitecture of bone by comparing the microarchitecture of men who were severely hypogonadal with that of matched eugonadal men using the μ MRI-based virtual bone biopsy.

Abbreviations: CT, Computed tomography; FOV, field of view; μ MRI, magnetic resonance microimaging; NEX, number of excitations; TR/TE, repetition time/echo time.

Subjects and Methods

Subjects

Each subject gave written informed consent to a protocol that was approved by the Offices of Regulatory Affairs at the University of Pennsylvania and Children's Hospital of Philadelphia.

We selected 10 untreated hypogonadal men and 10 matched eugonadal men from among men ages 18–80 yr. The hypogonadal men were selected from the Endocrinology practice of the University of Pennsylvania on the basis of a serum testosterone concentration of less than 8.7 nmol/liter at 0800–1000 h on two occasions. All 10 men had secondary hypogonadism. One man had the prepubertal onset of hypogonadism, and the other nine had postpubertal onset (Table 1). The one man who had the prepubertal onset had been treated with testosterone beginning at age 15 yr for 10 yr and then discontinued it for 20 yr. The other subject who had been treated with testosterone previously had discontinued it for approximately 5 yr. The estimated duration of hypogonadism was more than 2 yr in all of the subjects. Four men had been diagnosed as having deficiencies of T₄ and/or cortisol; three were stably replaced (Table 1).

For each hypogonadal man, we selected a eugonadal man, recruited through advertisements in local media, matched to the hypogonadal man for race and for age within ± 10 yr, whose serum testosterone concentration was greater than 10.4 nmol/liter at 0800–1000 h on two occasions and whose bone mineral density at L1–L4 was within the mean ± 2 sd for his age. Men were excluded from both groups if they had been consuming less than 750 mg of calcium per day as determined by a food frequency questionnaire. One man in the hypogonadal group was taking phenytoin sodium; he was also taking vitamin D, and his serum concentration of 25-hydroxyvitamin D was midnormal. No other man in either group was taking any other medication, including high-dose glucocorticoids, or had any disease known to affect bone. No man in either group consumed an average of more than two alcoholic drinks a day. In the hypogonadal group, three smoked cigarettes at the time of the study, three smoked previously, and four never smoked. In the eugonadal group, the corresponding numbers were three, four, and three.

Bone mineral density

Bone mineral density was determined by dual energy x-ray absorptiometry using a Hologic QDR-4500A densitometer (Hologic, Inc., Bedford, MA) operating software version 9.80 D. Measurements were obtained of the spine in the anterior-posterior projection of L1–L4 and the right hip. The right side was used for densitometry of the hip because the right side was used for μ MRI of the tibia.

μ MRI

μ MRI was performed at the right distal tibia using a Signa 1.5 Tesla MRI scanner (GE Medical Systems, Milwaukee, WI) and a custom-designed receive-only radiofrequency phased array surface coil. The distal tibia was used because signal-to-noise limitations dictate the use of a peripheral site and because the presence of distinct anatomic landmarks facilitates the precise location of the scan and analysis volume.

Subjects were placed supine, feet first, into the scanner. The entire foot was immobilized using a Vacfix system placed around the lower foot and coil and secured to the gantry. The coil was placed on the anterior right tibia, using the alignment light of the scanner to place the distal edge of the coil 1 cm proximal to the midpoint of the medial malleolus. The imaging protocol was similar to the one described for the distal radius (35). A series of axial localizer images was then acquired [field of view (FOV), 24 \times 24 cm²; repetition time/echo time (TR/TE), 300 msec/14 msec; matrix size, 256 \times 128; number of excitations (NEX), 0.75], from which the axial slice proximal to the distal tibia endplate was determined. From the chosen axial localizer slice, sagittal high-resolution localizer images were prescribed across the entire width of the tibia. The image showing the most proximal cortical endplate was chosen to prescribe the fast large-angle spin echo (FLASE) three-dimensional image series (FOV = 7 \times 5.25 cm²; TR/TE = 80 msec/9.7 msec; matrix = 512 \times 384 square pixels; slice thickness = 410 μ m, 32 slices; NEX = 1; flip angle = 140 degrees; scan time = 16.3 min). The distal boundary of the scan volume was located 8 mm from the distal cortical endplate of the tibia. The resulting acquisition voxel size was 137 \times 137 \times 410 μ m³. A typical high-resolution localizer image of the distal tibia and one of the cross-sectional high-resolution images are shown in Fig. 1.

The data were processed, as previously described (38), using a custom-designed processing package written in IDL (Interactive Data Language, Boulder, CO). The first step involved motion correction, followed by filtering and Fourier transformation of the data to yield 28 contiguous images (2 images on each side of the volume were discarded; Ref. 39). The volume of interest was selected manually on each of the 28 images by tracing a line approximately 1 mm from the endocortical boundary on the anterior half of the distal tibial metaphysis. The next step was computation of bone volume fraction (the fraction of the imaging voxel occupied by bone) maps (40). Finally, the images were subjected to subvoxel processing (41) to yield a voxel size of 69 \times 69 \times 103 μ m³.

Topological analysis of the trabecular network was performed on the entire volume of interest. The key step was the determination of the topological class of each image voxel. This process yielded the density of surface and curve voxels, as well as those that are part of mutual junctions. The topological analysis began with binarization of the three-dimensional images followed by skeletonization (36), which converted the platelike elements of the trabecular network to surfaces and the rodlike elements to curves. Each voxel was then classified as belonging to a curve, surface, or junction between these voxel types. In addition to the simple topological parameters, two composite parameters that have been found to be sensitive to bone loss (42) were calculated. One composite parameter was the surface/curve ratio, the ratio of all surface voxels to all curve voxels. The higher the ratio, the more intact is the trabecular network, and vice versa. The second composite parameter was the erosion index, a ratio of parameters that are expected to increase upon trabecular deterioration (curve edge and curve interior voxels, surface and profile edge voxels, and curve-curve junction voxels) to those expected to decrease (surface interior voxels and surface-surface

TABLE 1. Clinical information about the hypogonadal men

Patient no.	Age (yr)	Etiology of hypogonadism	Duration of hypogonadism (yr) ^a	Prior T treatment	Other hormonal deficiencies
1	31	Pinealoma	5	1 yr (5-4 yr ago)	T ₄ and cortisol, both replaced
2	46	Kallmann's syndrome	30	10 yr (30-20 yr ago)	
3	50	Lactotroph microadenoma	10		
4	52	Lactotroph microadenoma	5		
5	57	Nonfx pituitary macroadenoma	4		
6	60	Lactotroph microadenoma	2		
7	78	Lactotroph macroadenoma	5		T ₄ (primary hypothyroidism), replaced
8	48	Nonfx pituitary macroadenoma	2		T ₄ and cortisol, not replaced
9	68	Nonfx pituitary macroadenoma	6		
10	41	Nonfx pituitary macroadenoma	10		T ₄ and cortisol, both replaced

T, Testosterone; Nonfx, clinically nonfunctioning.

^a Estimated duration of hypogonadism.

FIG. 1. Anatomic site of μ MRI. *Left*, High-resolution sagittal image of the distal tibia. The *rectangle* encompasses the area from which data were collected. *Right*, One high-resolution cross-sectional slice through the tibia, aligned perpendicularly to the axis on the left, showing the trabecular architecture of the tibia. The *circle* shows the virtual bone biopsy core from which a three-dimensional projection image was derived. Two examples of three-dimensional projection images are shown in Fig. 2.

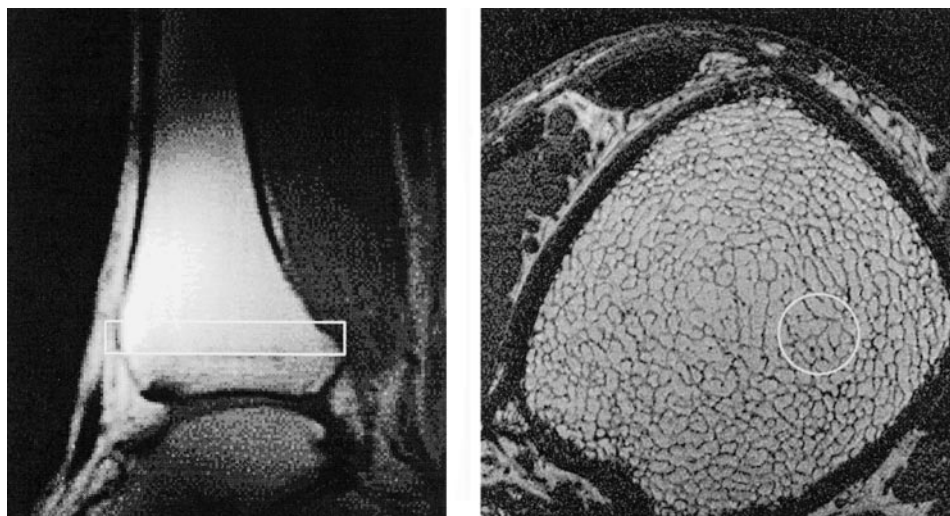


TABLE 2. Characteristics of the eugonadal and hypogonadal men

	Eugonadal men	Hypogonadal men	<i>P</i>
n	10	10	
Race	Caucasian, 8 African-American, 2	Caucasian, 8 African-American, 2	
Age (yr)	53.7 \pm 13.2	53.1 \pm 13.4	0.9
BMI (kg/m ²)	29.0 \pm 5.6	30.3 \pm 3.2	0.5
Calcium intake (mg/d)	1084 \pm 164	1175 \pm 248	0.3
Serum IGF-I (μ g/liter)	125 \pm 32	100 \pm 47	0.2
Serum estradiol [pg/ml (pmol/liter)]	19.7 \pm 3.4 (72 \pm 12)	8.9 \pm 4.5 (33 \pm 17)	0.0001
Serum testosterone [ng/dl (nmol/liter)]	522 \pm 126 (18.1 \pm 4.4)	88 \pm 51 (3.1 \pm 1.8)	0.0001

Results are given as mean \pm SD. BMI, Body mass index.

junctions). The higher the erosion index, the greater the degree to which the trabecular network has deteriorated.

This technique was validated in two ways. First, when μ MRI data were acquired at the distal tibia on three occasions in the same four normal subjects, the mean coefficients of variation for the surface/curve ratio and the erosion index were 5.3% and 4.5%, and the intraclass correlation coefficients were 0.93 and 0.91 (Weening, R. H., and F. W. Wehrli, unpublished observations). Second, μ MRI was performed on trabecular bone obtained from autopsy specimens at *in vitro* resolution (39 μ m), and then the images were resampled to yield images of *in vivo* resolution (156 μ m). In all parameters of trabecular architecture, the results at the two resolutions correlated highly with each other (38).

Statistical methods

Results are reported as mean \pm SD. Comparisons between the hypogonadal and eugonadal groups for all parameters were made using the paired *t* test and confirmed using the independent sample *t* test and Wilcoxon's signed rank test. Because the results were similar with all three tests, only the results of the paired *t* tests are reported. A type I error rate of 0.05 was used for determining statistical significance. JMP statistical software, version 4.0 (SAS Institute, Inc., Cary, NC), was used for all analyses.

Results

Characteristics of the hypogonadal and eugonadal men (Table 2)

The 10 hypogonadal and 10 eugonadal men, by design, were identical in racial composition and similar in mean age. They were also similar in mean body mass index and in calcium intake, which was normal. The mean serum IGF-I concentrations of the two groups were not significantly dif-

ferent. The mean serum estradiol concentration was significantly less in the hypogonadal men than in the eugonadal men. The mean serum testosterone concentration in the eugonadal men was midnormal (18.1 \pm 4.4 nmol/liter; range, 12.1–25.0 nmol/liter), and that in the hypogonadal men was severely subnormal (3.1 \pm 1.8 nmol/liter; range, 0.9–5.7 nmol/liter).

Bone mineral density (Table 3)

Mean bone mineral density of the spine, at L1–L4, in the hypogonadal men was 16% less than in the eugonadal men, but the difference was not statistically significant. Differences in mean bone mineral density for the total hip and three regional hip sites between the two groups were also not statistically significant.

Trabecular architecture as determined by μ MRI (Table 4)

The mean surface/curve ratio, which is the ratio of all surface voxels to all curve voxels and therefore is higher the more intact the bone, was 36% lower in the hypogonadal men than in the eugonadal men (*P* = 0.004). The mean erosion index, which is a composite ratio of topological parameters likely to increase to those likely to decrease when bone architecture deteriorates (see *Subjects and Methods* for a detailed definition) and is therefore higher the greater the deterioration, was 36% higher in the hypogonadal men than in the eugonadal men (*P* = 0.003). The bone volume fraction, which

is the fractional occupancy of voxels by bone, was 16% lower in hypogonadal men than in eugonadal men ($P = 0.001$). When these analyses were repeated after excluding the one man who had deficiencies of T_4 and cortisol that were not replaced and the one man taking phenytoin, the magnitude and statistical significance of the differences between the two groups in all parameters were even greater.

The ability of the μ MRI technique to discern individual trabeculae and the degree of trabecular deterioration is illustrated by three-dimensional projection images of virtual bone biopsies of the hypogonadal men compared with those

of the eugonadal men. Figure 2 shows projection images of the distal tibias of a 31-yr-old Caucasian hypogonadal man (subject 1 in Table 1) and a 28-yr-old Caucasian eugonadal man. The trabeculae of the eugonadal man exhibit a normal, predominantly plate-like network that is well connected, whereas the trabeculae of the hypogonadal man exhibit a greater number of rod-like elements, which are significantly disconnected.

Discussion

Previous studies have clearly demonstrated the association of male hypogonadism with decreased bone mineral density, but no previous studies have directly examined the effect of hypogonadism on the architecture of bone in humans. Some histomorphometric studies of men chosen for study because they had osteoporosis included men who were also hypogonadal (8, 9, 43), but none of these studies compared men chosen because they were hypogonadal with men chosen because they were eugonadal.

In this study, we used the technique of μ MRI to determine whether the trabecular architecture of men who have severe testosterone deficiency differs from that of eugonadal men matched for race and age. This technique permits quantitation of the degree to which trabecular plates (surfaces) have deteriorated to become rods (curves; Refs. 36–38), a change that characterizes osteoporosis (27, 44). We found that the surface/curve ratio at the distal tibia in the 10 hypogonadal men was 36% lower than that in the 10 eugonadal men, and, similarly, the erosion index in the hypogonadal men was 36% higher than that in the eugonadal men. Both of these differences were highly significant statistically, and both suggest much greater deterioration of trabecular architecture in the hypogonadal men. In contrast, there was not a statistically significant difference in bone mineral density of the spine and hip between the two groups.

The differences in architectural parameters between the hypogonadal and eugonadal men cannot be ascribed to differences in race, age, body mass index, calcium intake, or smoking because the two groups were quite similar in those parameters. It is also unlikely that the architectural differ-

TABLE 3. Bone mineral density of the eugonadal and hypogonadal men

	Eugonadal men	Hypogonadal men	<i>P</i>
n	10	10	
Spine, L1–L4	1.112 \pm 0.214	0.938 \pm 0.190	0.4
Hip, total	1.065 \pm 0.131	0.974 \pm 0.173	0.3
Femoral neck	0.847 \pm 0.101	0.797 \pm 0.139	0.5
Trochanter	0.814 \pm 0.119	0.717 \pm 0.141	0.2
Ward's triangle	0.670 \pm 0.151	0.591 \pm 0.169	0.4

The units for all bone mineral density values are g/cm^2 . Results are given as mean \pm SD.

TABLE 4. Parameters of trabecular architecture in eugonadal and hypogonadal men as assessed by μ MRI

	Eugonadal men	Hypogonadal men	<i>P</i>
n	10	10	
Surface/curve ratio ^a	10.8 \pm 2.4	6.9 \pm 1.8	0.004
Erosion index ^b	0.89 \pm 0.13	1.21 \pm 0.24	0.003
Bone volume fraction ^c	0.143 \pm 0.011	0.120 \pm 0.016	0.001

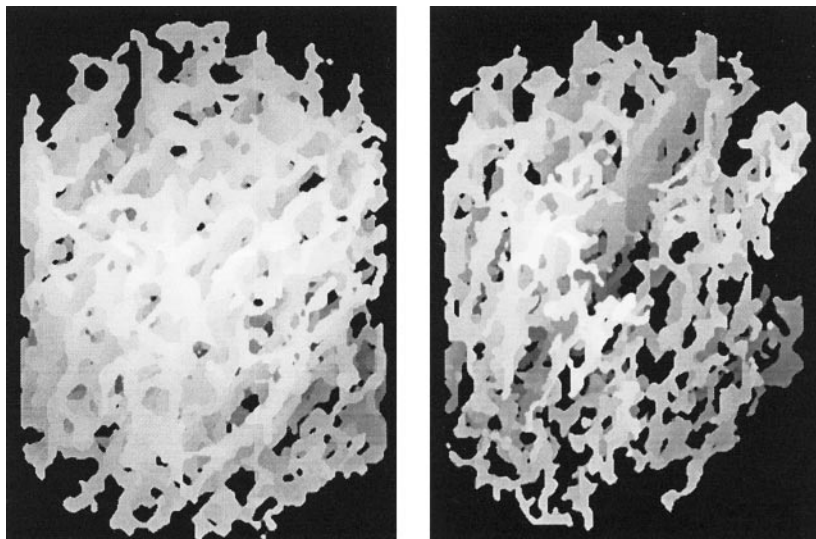
Results are given as mean \pm SD.

^a The surface/curve ratio is a ratio of all surface voxels (which represent trabecular plates) to all curve voxels (which represent rods). Higher values indicate a more intact trabecular network, and lower values indicate a network that has deteriorated more.

^b The erosion index is a ratio of parameters expected to increase when bone trabeculae deteriorate (voxel densities of curve interiors and edges, surface and profile edges, and curve-curve junctions) to those expected to decrease (densities of surface interior voxels and surface-surface junctions). Higher values indicate greater deterioration.

^c Bone volume fraction is the fractional occupancy of voxels by bone.

FIG. 2. Three-dimensional projection images of virtual bone biopsy cores of two men: a 28-yr-old, Caucasian eugonadal man (*left*) who was matched to a 31-yr-old, Caucasian hypogonadal man (*right*; subject 1 in Table 1). These images demonstrate the ability of the μ MRI technique to discern individual trabeculae. Note the well connected, predominantly platelike trabecular network of the eugonadal man on the *left* and the more disconnected, predominantly rodlike architecture of the hypogonadal man on the *right*.



ences between the two groups can be ascribed to hormonal differences other than those in gonadal steroids. Although four of the hypogonadal men had been diagnosed as having deficiencies of T₄ and cortisol, these deficiencies were stably replaced in three of the four. GH deficiency can contribute to decreased bone mineral density, and although the mean IGF-I values did not differ significantly between the two groups, we cannot exclude the possibility that GH deficiency contributed to the architectural deterioration in a few of the hypogonadal subjects. By far, the greatest hormonal difference between the two groups was in the serum testosterone concentrations, midnormal in the eugonadal men and severely subnormal in the hypogonadal men. The dramatically lower serum testosterone concentration in the hypogonadal men than in the eugonadal men, therefore, strongly suggests that this deficiency was a major contributing factor to deterioration of trabecular architecture in the hypogonadal men.

Estradiol was also lower in the hypogonadal men than in the eugonadal men, but it is not possible to determine from the design of this study the degree to which testosterone deficiency affected bone directly compared with the degree to which it acted indirectly via conversion to estradiol. From previous studies, testosterone appears to affect bone both directly as an androgen and via conversion to estradiol. Human chondrocytes (45), osteoblast-like cells (46), and human bone (47) express the androgen receptor. Androgens, even those that are not aromatizable to estrogens, stimulate cell division (48), increase androgen receptors (49), and stimulate mineralization in human osteoblast-like cells (50). Bone cells also express estrogen receptors, and men who either express a mutated estrogen receptor (51) or who cannot aromatize testosterone to estradiol (52–54) have osteoporosis and lack epiphyseal closure. Estradiol appears to contribute more to prevention of bone resorption than testosterone, but both appear to contribute equally to bone formation (55).

The potential significance of the architectural consequences in these hypogonadal men is that they may result in bone being less mechanically competent and therefore more susceptible to fracture. Several studies demonstrate that bone mass, or density, accounts for only about 40–60% of the mechanical strength of bone and that indices of bone architecture, as determined by high-resolution CT or MRI, account for an additional 25–40% (34, 56–58). Other studies demonstrate that bone architecture correlates well with vertebral deformities, better than bone density (21, 23, 38, 43).

The potential significance of these results can be questioned because the tibia, like the iliac crest from which physical bone biopsy specimens are taken, is a surrogate site. In this regard, a study comparing several sites rich in trabecular bone is of relevance (59). Trabecular bone in the spine was assessed longitudinally by quantitative CT and that in the radius and tibia were assessed by peripheral quantitative CT in women at several menopausal states. The rate of bone loss varied depending on the menopausal state, but at each of those states was quite similar in the three sites.

We conclude that hypogonadal men, compared with eugonadal men, exhibit a deterioration of trabecular architecture of the tibia, as determined by μ MRI. This deterioration may result in a decrease in bone strength to a greater degree than predicted by bone densitometry of the spine and hip.

Acknowledgments

We thank Helen Peachey, Louise Loh, Gail Jackson, and the nurses and staff of the General Clinical Research Center of the Hospital of the University of Pennsylvania for their assistance.

Received September 11, 2002. Accepted December 20, 2002.

Address all correspondence and requests for reprints to: Peter J. Snyder, M.D., 778 Clinical Research Building, 415 Curie Boulevard, Philadelphia, Pennsylvania 19104-6149. E-mail: pjs@pobox.upenn.edu.

This work was supported by National Institutes of Health Grants MO1-RR00041 (to the General Clinical Research Center, University of Pennsylvania), MO1-RR00240 (to the General Clinical Research Center, Children's Hospital of Philadelphia), R01 AR41443 and T32 CA74781 (to F.W.W.), and T32 AR07481 (to P.J.S.); and by a grant from the Endocrine Fellows Foundation (to M.B.).

References

- Orwoll ES, Klein RF 1995 Osteoporosis in men. *Endocr Rev* 16:87–116
- Cooper C, Atkinson EJ, O'Fallon WM, Melton 3rd LJ 1992 Incidence of clinically diagnosed vertebral fractures: a population-based study in Rochester, Minnesota, 1985–1989. *J Bone Miner Res* 7:221–227
- Nguyen TV, Eisman JA, Kelly PJ, Sambrook PN 1996 Risk factors for osteoporotic fractures in elderly men. *Am J Epidemiol* 144:255–263
- Myers AH, Robinson EG, Van Natta ML, Michelson JD, Collins K, Baker SP 1991 Hip fractures among the elderly: factors associated with in-hospital mortality. *Am J Epidemiol* 134:1128–1137
- Poor G, Atkinson EJ, O'Fallon WM, Melton 3rd LJ 1995 Determinants of reduced survival following hip fractures in men. *Clin Orthop* 319:260–265
- Kelepouris N, Harper KD, Gannon F, Kaplan FS, Haddad JG 1995 Severe osteoporosis in men. *Ann Intern Med* 123:452–460
- Seeman E, Melton LJI, O'Fallon WM, Riggs B 1983 Risk factors for spinal osteoporosis in men. *Am J Med* 75:977–983
- Delichatsios HK, Lane JM, Rivlin RS 1995 Bone histomorphometry in men with spinal osteoporosis. *Calcif Tissue Int* 56:359–363
- Jackson JA, Kleerekoper M, Parfitt AM, Rao DS, Villanueva AR, Frame B 1987 Bone histomorphometry in hypogonadal and eugonadal men with spinal osteoporosis. *J Clin Endocrinol Metab* 65:53–58
- Devogelaer JP, De Cooman S, Nagant de Deuxchaisnes C 1992 Low bone mass in hypogonadal males. Effect of testosterone substitution therapy, a densitometric study. *Maturitas* 15:17–23
- Katznelson L, Finkelstein JS, Schoenfeld DA, Rosenthal DI, Anderson EJ, Klibanski A 1996 Increase in bone density and lean body mass during testosterone administration in men with acquired hypogonadism. *J Clin Endocrinol Metab* 81:4358–4365
- Stepan JJ, Lachman M, Zverina J, Pacovsky V, Baylink DJ 1989 Castrated men exhibit bone loss: effect of calcitonin treatment on biochemical indices of bone remodeling. *J Clin Endocrinol Metab* 69:523–526
- Goldray D, Weisman Y, Jaccard N, Merdler C, Chen J, Matzkin H 1993 Decreased bone density in elderly men treated with the gonadotropin-releasing hormone agonist decapeptyl (D-Trp6-GnRH). *J Clin Endocrinol Metab* 76:288–290
- Kiratli BJ, Srinivas S, Perkash I, Terris MK 2001 Progressive decrease in bone density over 10 years of androgen deprivation therapy in patients with prostate cancer. *Urology* 57:127–132
- Stoch SA, Parker RA, Chen L, Buble G, Ko YJ, Vincelette A, Greenspan SL 2001 Bone loss in men with prostate cancer treated with gonadotropin-releasing hormone agonists. *J Clin Endocrinol Metab* 86:2787–2791
- Behre HM, Kliesch S, Leifke E, Link TM, Nieschlag E 1997 Long-term effect of testosterone therapy on bone mineral density in hypogonadal men. *J Clin Endocrinol Metab* 82:2386–2390
- Finkelstein JS, Klibanski A, Neer RM, Doppelt SH, Rosenthal DI, Segre GV, Crowley WF 1989 Increases in bone density during treatment of men with idiopathic hypogonadotropic hypogonadism. *J Clin Endocrinol Metab* 69:776–783
- Snyder PJ, Peachey H, Berlin JA, Hannoush P, Haddad G, Dlewati A, Santanna J, Loh L, Lenrow DA, Holmes JH, Kapoor SC, Atkinson LE, Strom BL 2000 Effects of testosterone replacement in hypogonadal men. *J Clin Endocrinol Metab* 85:2670–2677
- Mann T, Oviatt SK, Wilson D, Nelson D, Orwoll ES 1992 Vertebral deformity in men. *J Bone Miner Res* 7:1259–1265
- Marshall D, Johnell O, Wedel H 1996 Meta-analysis of how well measures of bone mineral density predict occurrence of osteoporotic fractures. *BMJ* 312:1254–1259
- Kleerekoper M, Villanueva AR, Stanciu J, Rao DS, Parfitt AM 1985 The role of three-dimensional trabecular microstructure in the pathogenesis of vertebral compression fractures. *Calcif Tissue Int* 37:594–597
- Legrand E, Chappard D, Basle MF, Audran M 1999 Evaluation of trabecular

- microarchitecture. Prospects for predicting the risk of osteoporosis and fracture. *Rev Rhum Engl Ed* 66:543–547
23. Recker RR 1993 Architecture and vertebral fracture. *Calcif Tissue Int* 53: S139–S142
 24. Chesnut 3rd CH, Silverman S, Andriano K, Genant H, Gimona A, Harris S, Kiel D, LeBoff M, Maricic M, Miller P, Moniz C, Peacock M, Richardson P, Watts N, Baylink D 2000 A randomized trial of nasal spray salmon calcitonin in postmenopausal women with established osteoporosis: the prevent recurrence of osteoporotic fractures study. PROOF Study Group. *Am J Med* 109: 267–276
 25. Sarkar S, Mitlak BH, Wong M, Stock JL, Black DM, Harper KD 2002 Relationships between bone mineral density and incident vertebral fracture risk with raloxifene therapy. *J Bone Miner Res* 17:1–10
 26. Riggs BL, Melton 3rd LJ 2002 Bone turnover matters: the raloxifene treatment paradox of dramatic decreases in vertebral fractures without commensurate increases in bone density. *J Bone Miner Res* 17:11–14
 27. Parfitt AM, Mathews CH, Villanueva AR, Kleerekoper M, Frame B, Rao DS 1983 Relationships between surface, volume, and thickness of iliac trabecular bone in aging and in osteoporosis. Implications for the microanatomic and cellular mechanisms of bone loss. *J Clin Invest* 72:1396–1409
 28. Dambacher MA, Neff M, Kissling R, Qin L 1998 Highly precise peripheral quantitative computed tomography for the evaluation of bone density, loss of bone density and structures. Consequences for prophylaxis and treatment. *Drugs Aging* 12:15–24
 29. Gordon CL, Lang TF, Augat P, Genant HK 1998 Image-based assessment of spinal trabecular bone structure from high-resolution CT images. *Osteoporos Int* 8:317–325
 30. Laib A, Rueggsegger P 1999 Calibration of trabecular bone structure measurements of *in vivo* three-dimensional peripheral quantitative computed tomography with 28-micron-resolution microcomputed tomography. *Bone* 24:35–39
 31. Chung H, Wehrli FW, Williams JL, Kugelmass SD 1993 Relationship between NMR transverse relaxation, trabecular bone architecture, and strength. *Proc Natl Acad Sci USA* 90:10250–10254
 32. Chung HW, Wehrli FW, Williams JL, Wehrli SL 1995 Three-dimensional nuclear magnetic resonance microimaging of trabecular bone. *J Bone Miner Res* 10:1452–1461
 33. Majumdar S, Genant HK, Grampp S, Newitt DC, Truong VH, Lin JC, Mathur A 1997 Correlation of trabecular bone structure with age, bone mineral density, and osteoporotic status: *in vivo* studies in the distal radius using high resolution magnetic resonance imaging. *J Bone Miner Res* 12:111–118
 34. Majumdar S, Kothari M, Augat P, Newitt DC, Link TM, Lin JC, Lang T, Lu Y, Genant HK 1998 High-resolution magnetic resonance imaging: three-dimensional trabecular bone architecture and biomechanical properties. *Bone* 22:445–454
 35. Wehrli FW, Hwang SN, Ma J, Song HK, Ford JC, Haddad JG 1998 Cancellous bone volume and structure in the forearm: noninvasive assessment with MR microimaging and image processing. *Radiology* 206:347–357
 36. Saha PK, Gomberg BR, Wehrli FW 2000 Three-dimensional digital topological characterization of cancellous bone architecture. *Int J Imag Syst Tech* 11:81–90
 37. Wehrli FW, Hopkins JA, Hwang SN, Song HK, Snyder PJ, Haddad JG 2000 Cross-sectional study of osteopenia with quantitative MR imaging and bone densitometry. *Radiology* 217:527–538
 38. Wehrli FW, Gomberg BR, Saha PK, Song HK, Hwang SN, Snyder PJ 2001 Digital topological analysis of *in vivo* magnetic resonance microimages of trabecular bone reveals structural implications of osteoporosis. *J Bone Miner Res* 16:1520–1531
 39. Song HK, Wehrli FW 1999 *In vivo* micro-imaging using alternating navigator echoes with applications to cancellous bone structural analysis. *Magn Reson Med* 41:947–953
 40. Hwang SN, Wehrli FW 1999 Estimating voxel volume fractions of trabecular bone on the basis of magnetic resonances acquired *in vivo*. *Int J Imag Syst Tech* 10:186–198
 41. Hwang SN, Wehrli FW 2002 Subvoxel processing: a method for reducing partial volume blurring with application to *in vivo* MR images of trabecular bone. *Magn Reson Med* 47:948–957
 42. Gomberg BR, Saha PK, Song HK, Hwang SN, Wehrli FW 2000 Topological analysis of trabecular bone MR images. *IEEE Trans Med Imaging* 19:166–174
 43. Legrand E, Chappard D, Pascaretti C, Duquenne M, Krebs S, Rohmer V, Basle MF, Audran M 2000 Trabecular bone microarchitecture, bone mineral density, and vertebral fractures in male osteoporosis. *J Bone Miner Res* 15: 13–19
 44. Compston JE, Mellish RW, Garrahan NJ 1987 Age-related changes in iliac crest trabecular microanatomic bone structure in man. *Bone* 8:289–292
 45. Carrascosa A, Audi L, Ferrandez MA, Ballabriga A 1990 Biological effects of androgens and identification of specific dihydrotestosterone-binding sites in cultured human fetal epiphyseal chondrocytes. *J Clin Endocrinol Metab* 70: 134–140
 46. Colvard DS, Eriksen EF, Keeting PE, Wilson EM, Lubahn DB, French FS, Riggs BL, Spelsberg TC 1989 Identification of androgen receptors in normal human osteoblast-like cells. *Proc Natl Acad Sci USA* 86:854–857
 47. Abu EO, Horner A, Kusec V, Triffitt JT, Compston JE 1997 The localization of androgen receptors in human bone. *J Clin Endocrinol Metab* 82:3493–3497
 48. Kasperk CH, Wergedal JE, Farley JR, Linkhart TA, Turner RT, Baylink DJ 1989 Androgens directly stimulate proliferation of bone cells *in vitro*. *Endocrinology* 124:1576–1578
 49. Wren K, Keenan E, Zhang X, Ramsey B, Orwoll E 1999 Homologous androgen receptor up-regulation in osteoblastic cells may be associated with enhanced functional androgen responsiveness. *Endocrinology* 140:3114–3124
 50. Takeuchi M, Kakushi H, Tohkin M 1994 Androgens directly stimulate mineralization and increase androgen receptors in human osteoblast-like osteosarcoma cells. *Biochem Biophys Res Commun* 204:905–911
 51. Smith EP, Boyd J, Frank GR, Takahashi H, Cohen RM, Specker B, Williams TC, Lubahn DB, Korach KS 1994 Estrogen resistance caused by a mutation in the estrogen-receptor gene in a man. *N Engl J Med* 331:1056–1061
 52. Bilezikian JP, Morishima A, Bell J, Grumbach MM 1998 Increased bone mass as a result of estrogen therapy in a man with aromatase deficiency. *N Engl J Med* 339:599–603
 53. Carani C, Qin K, Simoni M, Faustini-Fustini M, Serpente S, Boyd J, Korach KS, Simpson ER 1997 Effect of testosterone and estradiol in a man with aromatase deficiency. *N Engl J Med* 337:91–95
 54. Morishima A, Grumbach MM, Simpson ER, Fisher C, Qin K 1995 Aromatase deficiency in male and female siblings caused by a novel mutation and the physiological role of estrogens. *J Clin Endocrinol Metab* 80:3689–3698
 55. Falahati-Nini A, Riggs BL, Atkinson EJ, O'Fallon WM, Eastell R, Khosla S 2000 Relative contributions of testosterone and estrogen in regulating bone resorption and formation in normal elderly men. *J Clin Invest* 106:1553–1560
 56. Gordon CL, Webber CE, Nicholson PS 1998 Relation between image-based assessment of distal radius trabecular structure and compressive strength. *Can Assoc Radiol J* 49:390–397
 57. Oden ZM, Selvitelli DM, Hayes WC, Myers ER 1998 The effect of trabecular structure on DXA-based predictions of bovine bone failure. *Calcif Tissue Int* 63:67–73
 58. Ulrich D, van Rietbergen B, Laib A, Rueggsegger P 1999 The ability of three-dimensional structural indices to reflect mechanical aspects of trabecular bone. *Bone* 25:55–60
 59. Ito M, Nakamura T, Tsurusaki K, Uetani M, Hayashi K 1999 Effects of menopause on age-dependent bone loss in the axial and appendicular skeletons in healthy Japanese women. *Osteoporos Int* 10:377–383